RESEARCH

Composite Nanoarchitectonics of Poly(lactic acid)/Metal Organic Framework with Property Investigations Toward Packaging Applications

Badiaa Bouider[1] · Boubkeur Seddik Bouakaz[1] · Slimane Haffad[1] · Abdelkader Berrayah[2] · Anthony Magueresse[3] · Yves Grohens[4] · Abderrahmane Habi[1]

Abstract

In this study, poly(lactic acid) (PLA), metal organic framework (MOF-5) and metal organic framework/graphene oxide (MOF-5/GO) were associated to prepare nanocomposites through melt extrusion method using a vertical co-rotating twin-screw micro compounder. GO, MOF-5 and MOF-5/GO composites were synthesized, respectively, using the modified Hummer's method, facile method at room temperature and in situ incorporation of GO into MOF-5 precursors. PLA and MOF nanocomposites were obtained with the incorporation of 3 and 5% w/w of MOF-5 and MOF-5/GO nanofillers into the PLA matrix. The morphological, rheological, thermal, impact tests and barrier properties of the composites were evaluated by Fourier transform infrared spectroscopy (FT-IR), X-ray diffraction (XRD), scanning electron microscopy (SEM), thermogravimetric analysis (TGA), differential scanning calorimetry (DSC), impact resistance tests and water vapor permeability test (WVP). According to the XRD results, MOF-5 and MOF-5/GO composites were successfully incorporated into the PLA matrix without altering the crystal structure of the MOF-5 and MOF-5/GO composites. The SEM images and FT-IR spectra indicate that MOF-5 and MOF-5/GO fillers are compatibles with PLA matrix. In the rheological study, the non-terminal behavior observed for PLA nanocomposites indicates pseudo-solid behavior, characteristic of a good dispersion state of the used nanofillers. The decrease in cold crystallization enthalpy indicates a high potential of these materials in various applications including gas separation, energy and packaging. Water vapor permeations (WVP) were strongly reduced by the incorporation of MOF-5/GO, and the better results are obtained with PLA/MOF-5/GO containing 5 mass% of MOF-5/GO-5. The results indicate that the structure–properties relationship is established and packaging application can be considered for these materials.

Keywords Poly(lactic acid) · Metal organic framework · Nanocomposites · Packaging

1 Introduction

Due to their inherent qualities, polymer materials are now utilized more often in a variety of industries (packing, transportation, health, etc.) and in all technologies that make daily life easier for humans. The extensive usage of these materials has led to significant management issues with respect to the buildup of non-biodegradable trash. In fact, even though plastic materials are incredibly simple to make, they are considerably harder to get rid of in the environment. Scientists focus heavily on the creation and synthesis of novel biodegradable materials, which are more considerate of the environment, in order to address and mitigate the effects of traditional plastic material that is not biodegradable [1–3].

✉ Abderrahmane Habi
abderrahmane.habi@univ-bejaia.dz; abderhabi@yahoo.fr

1   Laboratoire des Matériaux Organiques, Faculté de Technologie, Université de Bejaia, 06000 Bejaia, Algeria

2   Laboratoire de Recherche sur les Macromolécules, Faculté des Sciences, Université Aboubakr Belkaïd, Tlemcen, Algeria

3   Centre de recherche Christiaan Huygens, IRDL CNRS 6027, Rue de St Maudé, BP 92116, 56321 Lorient, France

4   COMPOSITIC, Université de Bretagne-Sud, 2 Allée Copernic, 56270 Ploemeur, France

Biopolymers are a group of organic polymers that are easily biodegradable. Like other polymers, biopolymers are monomeric units covalently clubbed together to form bigger molecules. Among the various biopolymers, poly(lactic acid) (PLA), a lactic acid (LA) based biopolymer, is a thermoplastic polyester that is widely developed and have received great attention from the scientific community due to the global environmental concerns and their use as an alternative to polymer materials of petrochemical origin [4–6]. PLA, a biodegradable aliphatic polyester of significant importance well suited for the production of disposable materials, is typically prepared from fermented plant starch, such as wheat starch, potato starch, sweet potato starch, cornstarch, and dextrin [7, 8].

The packaging industry has recently become interested to PLA due to its durable, good tensile strength, biocompatibility and biodegradable properties [9]. It should be noticed that since PLA is a semi-crystalline polymer, the amount of the crystalline portion has a significant effect on the subsequent mechanical properties. The percent crystallinity of PLA and its nanocomposites strongly depend on the thermal history [10]. To improve the PLA properties and overcome its disadvantages such as low thermal stability and low process ability, several studies have been carried out using fillers such as clay minerals, carbon nanotubes, graphene and silica to obtain polymer nanocomposites materials [11–14].

Polymer nanocomposites offer significantly improved properties compared with traditional polymer matrices or composites [15, 16] and are therefore used in numerous applications such as water treatment [17]. Otherwise, it is well known that incorporating organically modified montmorillonite leads to improving polymer blend's properties which can be used in packaging [18–20]. Lamellar filler, of the same type as montmorillonite, called graphene, has been used in the past years to improve the polymer's properties. Graphene exhibits unique two-dimensional (2D) sp^2 hybridized construction where carbon atoms placed in a hexagonal lattice, composed of one atom thick planar sheet. This unusual structure of graphene has attracted much interest and led to outstanding physicochemical characteristics [21]. When 2D graphene and its hybrid derivatives are mixed with polymers, hybrid/nanocomposites may be created undergo stimulus-induced optical and electrical changes which are important for many new switchable device technologies [22, 23] such as, detection of aromatic volatile organic compounds [24], optoelectronic, energy, and biological applications [23] and electrochemical sensors [25]. Issaadi et al. [15] studied PLA/MA-g-PLA/GFe nanocomposites and showed that the addition of 7% by weight of epoxy graphene was sufficient to improve the thermal, rheological, mechanical and barrier properties of PLA matrix.

Recently, the use of metal organic frameworks (MOFs) and MOF/graphene oxide (MOF/GO) has received more attention due to their facile synthesis, larger surface area, adsorption properties and catalysis [26]. An extensive range of applications, including CO_2 capture, gas separation and photocatalysis, have brought attention to MOF/GO composites [27–29]. MOFs are porous crystalline materials that have been emerged recently. They are hybrid materials made up of a mixture of organic molecules linked to metallic species giving rise to a new structure with different properties [30, 31]. This combination of transition metals coordinated by organic linked creates a porous structure in one, two or three dimensions [32]. MOFs have several characteristics such as porosity, ultrahigh specific surface area, and biocompatibility [31].

The researchers are interested in the MOF/GO formation method. Petit and Bandosz [33] describe the mechanism as follows: In MOF-5, benzene carboxylates (1, 4 benzenedicarboxylate) create connections between the $[Zn_4O]^{6+}$ tetrahedra that occupy the corners of a basic cubic structure. The resultant substance has the formula Zn_4O (H-BDC)$_3$. Since GO contains epoxy and carboxylic groups, it is anticipated that these groups may serve as an anchor for zinc oxide clusters. First, MOF-5 "'blocks'" react with epoxy groups on GO to adhere to a graphene layer. This may occur in a manner akin to the way that water interacts with MOF-5. A crucial stage in the disintegration of MOF-5 in water is the substitution of oxygen atoms in ZnO_4 tetrahedra with oxygen atoms from water. In the case of MOF-5/GO, the epoxy groups on GO's oxygen atoms are supposed to function similarly to water's oxygen atoms.

Fabrication of polymer–MOF mixed matrix membranes (MMMs) is motivated by the ease of processing, cost effectiveness, and great selectivity of MOF particles [34]. The preparation of MMM made of PLA/MOF is one of the materials for the purification of air and water [35]. These membranes can be used in packaging to maintain the ideal concentration of CO_2, organic compounds, or other gases in a package's headspace, which might affect the performance of the package [36].

Only a few studies have been published on PLA/MOFs composites to improve the thermal, mechanical and permeability properties of the PLA polymer matrix [36–39]. Kathuria et al. [36–38] studied PLLA/MOF Cu$_3$(BTC)$_2$ and demonstrated that PLLA and MOF Cu$_3$ (BTC)$_2$ have a strong interfacial interactions that played an important role in enhancing the toughness and CO_2 permeability coefficient of PLA/MOF composites. Dai et al. [39, 40] reported that tensile strength and rupture strength of PLA/ZIF-8 membrane increases at 5.02 MPa and 88.81%, compared to 2.77 MPa and 57.89% for pure PLA membranes. In addition, the incorporation of ZIF-8/GO nanoparticles leads to an improvement and significant increase in tensile strength.

In our previous work, two nanofillers MOF-5 and MOF-5/GO were synthesized and characterized by means

of X-ray diffraction (XRD), Fourier transform infrared spectroscopy (FT-IR) and thermal gravimetric analysis (TGA) [29]. The main objective of this study is the use of these two nanofillers to fabricate binary and ternary nanocomposites based on PLA for use in packaging domain. MOF-5 and MOF-5/GO nanofillers were melt-blended with PLA matrix at different percentage and their effects on the morphology, thermal stability, rheological and barrier properties of PLA were examined.

2 Experimental Part

2.1 Materials

The materials used in this study are all commercially available reagents and used directly without prior purification. Terephthalic acid [1, 4-benzenedicarboxylic acid, (H$_2$BDC), Biochem, 99.0%], zinc acetate dihydrate [Zn(OAc)$_2$·2H$_2$O, Labosi], chloroform (CHCl$_3$) (99.5%) and N, N-dimethylformamide (DMF) were purchased from Biochem, potassium permanganate (Biochem, 99% purity), hydrogen peroxide (Sialchim, 35% purity), hydrochloric acid (Samchun Chemical, 35.0–37.0%), Sulfuric acid (Sigma Aldrich, 98% purity) and graphite powder with a diameter less than 20 μm were purchased from Sigma Aldrich. It should be noticed that deionized (DI) water was used in all experiments.

The PLA (7001D) is a commercial product of Nature Works Co, Ltd. This material has a density of 1.24 g/cm^3, a glass transition temperature of 55–60 °C, and a melting temperature of 154 °C. The molecular weight of the material is 113,000 g/mol.

2.2 Sample Preparation

2.2.1 Synthesis of MOF-5

MOF-5 was prepared by a facile method at room temperature according to the method reported by Yaghi et al. [29, 30]. Briefly, 5 g of terephthalic acid and 8.5 mL of triethylamine were dissolved in 400 mL of DMF. The zinc salt solution was prepared using 16.9 g of zinc acetate di-hydrate [Zn(OAc)$_2$·2H$_2$O] was dissolved in 500 mL of DMF. The zinc salt solution was added to the organic solution with stirring for 15 min, forming a white precipitate and the mixture was stirred 2 h 30 min. The precipitate was filtered and soaked in 250 mL of DMF overnight. It was then filtered again and immersed in 350 mL of chloroform. The solvent was exchanged 3 times over 7 days. After decantation the final product was collected and dried 2 h at 120 °C.

2.2.2 Preparation of MOF-5/GO Composites

GO was prepared from natural graphite (20 μm) according to the Hummer modifier method [41, 42]. The MOF-5/GO composite was synthesized by the in situ growth method previously reported [29, 43]. Briefly, a quantity of parboiled GO (a mass amount of 5 or 10 wt% relative to the yield of pure MOF) was dispersed in 40 mL of DMF and sonicated for 2 h. The GO suspension was then added to the MOF-5 reaction medium. Finally, the final product was filtered and washed by DMF. For brevity, the resulting composites are abbreviated to as MOF-5/GO-5, and MOF-5/GO-10, where 5 and 10 represent the weight fraction % of GO in the samples, respectively.

2.2.3 Preparation of PLA/Nanocomposites

Before use, the PLA as well as the nanofillers were dried at 60 °C for 24 h to eliminate residual moisture and avoid all types of degradation during processing in the molten state. Appropriate quantities (14 g) of PLA and nanofillers (3% and 5%) were introduced into a machine (5 and 15 Micro Compounder DSM Xplore Model 2005 twin-screw extruder) to fabricate hybrid materials. The equipment was previously programmed to operate at a temperature of 180 °C and a rotation speed of 80 rpm for 6 min [13]. For brevity, the samples containing 3 and 5 wt% of MOF-5/GO-5 are abbreviated as PMG53, PMG55, and the samples containing 3 and 5 wt% of MOF-5/GO-10 are abbreviated as PMG103, PMG105.

2.2.4 Films Preparation

The impact tests were carried out on samples in the form of bars obtained using a Mitsubishi type press, consisting of two heating plates connected to a cold water circuit for cooling. A pressure of 1 bar and a temperature of 180 °C were applied for 3 min. The same procedure was used to prepare films about 160 μm thick and 230 mm in diameter. For this purpose, 4 g of each formulation were placed under a pressure of 1 bar and a compression force of 0.5 ton (Fig. 1).

2.3 Characterizations

FT-IR spectroscopic analysis was performed using an FT-IR-8400S spectrometer, from Shimadzu, Japan. The spectra were recorded from 400 to 4000 cm^{-1} with a resolution of 1 cm^{-1}. Thin films of PLA, PLA/MOF-5 and PLA/MOF-5/GO were prepared and analyzed in transmission mode.

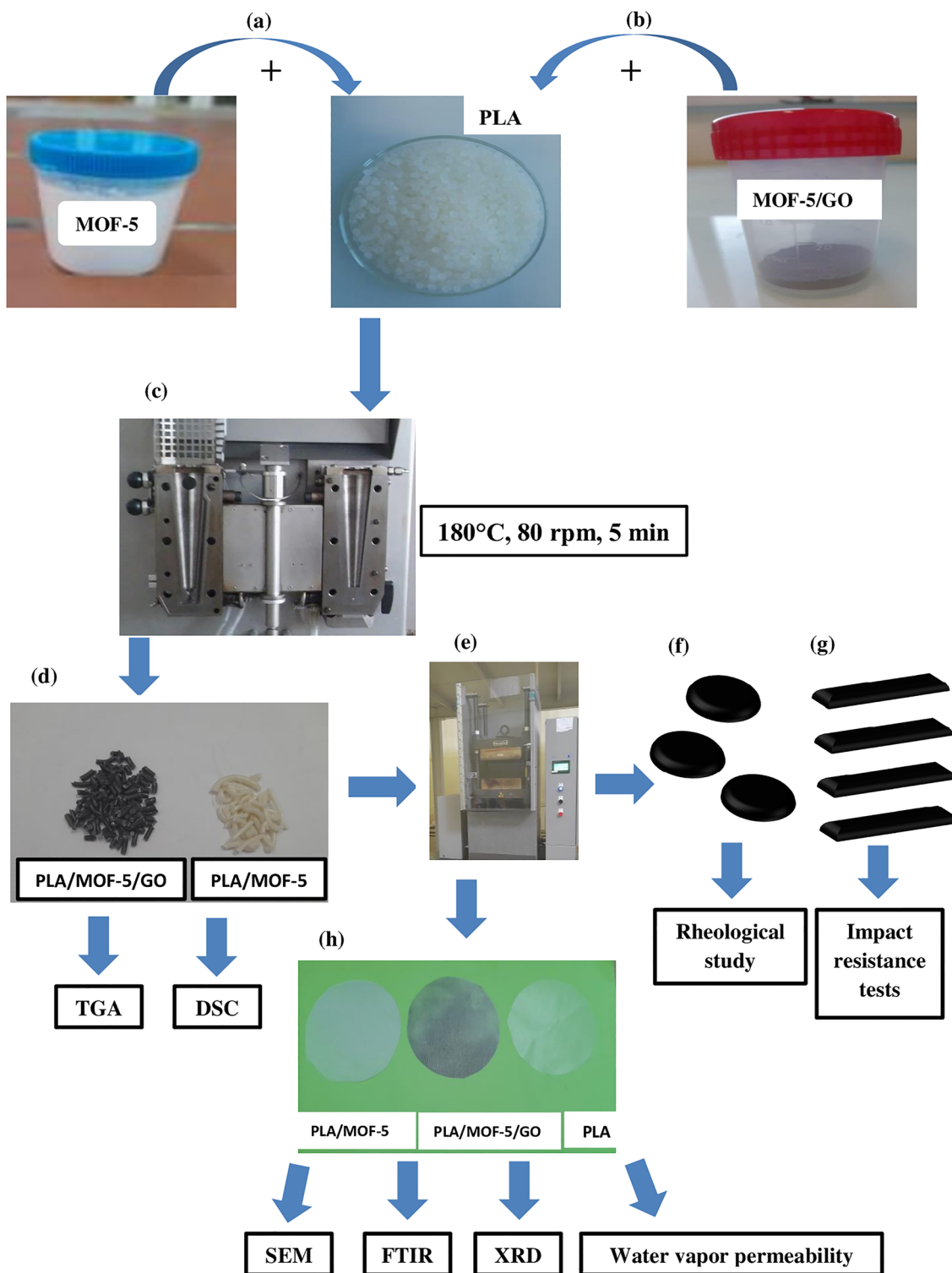The XRD study of the samples was carried using an Empyrean Diffractometer at 45 kV and 40 mA (1600 W)

Fig. 1 Schematic illustration of the preparation of nanocomposites (a) elaboration of PLA/MOF-5, (b) elaboration of PLA/MOF-5/GO, (c) vertical co-rotating twin-screw micro compounder, (d) extrudates, (e) press, (f) disks, (g) bars, and (h) film of nanocomposites

with monochromatic Cu Kα radiation (λ = 1.5406 Å). Measurements were made in the range of 5° to 45° of 2θ with a scan step of 0.02°.

The morphology of the fractured samples of the PLA, PLA/MOF-5 and PLA/MOF-5/GO nanocomposites films were observed using a JSM-IT500HR scanning electron

microscope. The micrographs were collected from the secondary electron images obtained with energy of 3 kV.

The storage modulus (G′), the loss modulus (G″) and the complex viscosity (η*) were measured as a function of the angular frequency (ω) using a Discovery HR-2 Rheometer in the dynamic oscillatory mode with parallel plate geometry of 25 mm diameter. Before the measurements, the bars already prepared were dried at 60 °C under vacuum for 24 h and the various parameters were measured in the linear domain at 180 °C with a gap of 900 μm, frequencies ranging from 0.01 to 100 Hz and under a deformation of 1%. For each material, three tests were made to verify the reproducibility of the results.

The thermal stability of the materials studied was evaluated using the Linseis equipment (STA PT 1600). TGA analyzes was performed from 30 to 600 °C at a heating rate of 10 °C/min under nitrogen flow. The masses of the samples were between 15 and 20 mg. Values are presented as averages ±2%/°C standard error.

The thermal characterizations by DSC were carried out using a DSC Q2000 (TA Instruments, New Castle, DE, USA). A heating/cooling/heating procedure was applied over a temperature range from 20 to 200 °C at 20 °C/min under atmospheric nitrogen (N_2). Glass transition temperature (T_g), crystallization temperature (T_c), melting temperature (T_m), and enthalpy of melting (ΔH_m) were determined from the second heating scans. The degree of crystallinity of PLA and its nanocomposites was calculated by the Eq. (1):

$$X_c = \frac{\Delta H_m}{\Delta H_m^{\circ} * (1 - \Phi)}, \tag{1}$$

where ΔH_m represents the heat of fusion (J/g), ΔH_m° represents the theoretical heat of fusion of 100% crystalline PLA (93.60 J/g) [2] and Φ represents the mass fraction of the nanofillers in the nanocomposites. Values are presented as averages ±0.02 standard error.

The impact tester (Testing Machines, Inc., Ronkonkoma, NY, USA) was used to measure Izod impact strength on unnotched bars of dimensions ($6.3 \times 1.3 \times 0.2$ cm) of four samples for each treatment under ambient conditions, in accordance with ASTM D256-10.

The permeability tests were carried out using the "cups method", referring to the ISO 7783 standard, on films having a thickness of approximately 160 μm. This method consists in following the evolution of the permeameter mass as a function of time, in a controlled environment (T = 23 °C ±1°C, humidity = 48% ±2%, RH). This permeameter is a cylindrical aluminum tank, containing 10 g of anhydrous salt [calcium chloride ($CaCl_2$)] and sealed with the film to be tested. Mass measurements were taken regularly to control the evolution of the mass of the salt

(corresponding to its water uptake). Finally, the permeability rate values were calculated by Eq. (2):

$$WVP = \frac{\Delta M \times e}{A \times \Delta t \times \Delta P}, \tag{2}$$

where WVP is the water vapor permeability coefficient, m (g) is the gain of mass, e (m) is the film thickness, A (m^2) is area of the film separating the inside of the tank and the outside, t (s) is the time and ΔP (Pa) is pressure difference between upstream and downstream of the film. From the experimental conditions, the water vapor ΔP is 1400.3 Pa calculated for a temperature of 23 °C and a relative humidity of 48% [11].

3 Results and Discussion

3.1 Study of Morphology

3.1.1 Fourier Transform Infrared Spectroscopy (FT-IR)

FT-IR spectrum analysis is an effective analytical technique that makes it possible to highlight the existence of functional groups and to study the interactions between the MOF-5 and/or MOF-5/GO particles and the PLA matrix. The FT-IR spectra of pure PLA and the PLA-based nanocomposites filled with MOF-5 and MOF-5/GO are presented in Fig. 2a. It can be seen that no changes are apparent except in the carbonyl range where the corresponding picks shifted to lower wavenumbers as illustrated in Fig. 2b. Indeed, the characteristic peak of the carbonyl groups of PLA located at 1755 cm^{-1} is shifted to 1721 cm^{-1} in the case of the nanocomposite containing 3% MOF-5 while that of the nanocomposite with 5% MOF-5 is shifted to 1719 cm^{-1}. This result attributed to the existence of specific interactions between the C=O groups of PLA and the Zn^{2+} of MOF-5 reflects the good compatibility between the PLA matrix and the MOF-5 nanofiller [39, 40].

The FT-IR spectra of the PLA/MOF-5/GO-5 and PLA/MOF-5/GO-10 nanocomposites show that the characteristic carbonyl peaks are shifted towards the lower wavenumbers. However, it should be noticed that the shift of the carbonyl peaks is significantly greater in the case of the MOF-5/GO-5 nanocomposite compared to the MOF-5/GO-10 nanocomposite. These observations confirm the formation of hydrogen bonds between the MOF-5/GO nanofillers and the PLA matrix [40, 44] indicating a good compatibility between them.

3.1.2 X-Ray Diffraction (XRD)

XRD makes it possible to evaluate, in the case of nanocomposites, the state of dispersion of the nanofiller within
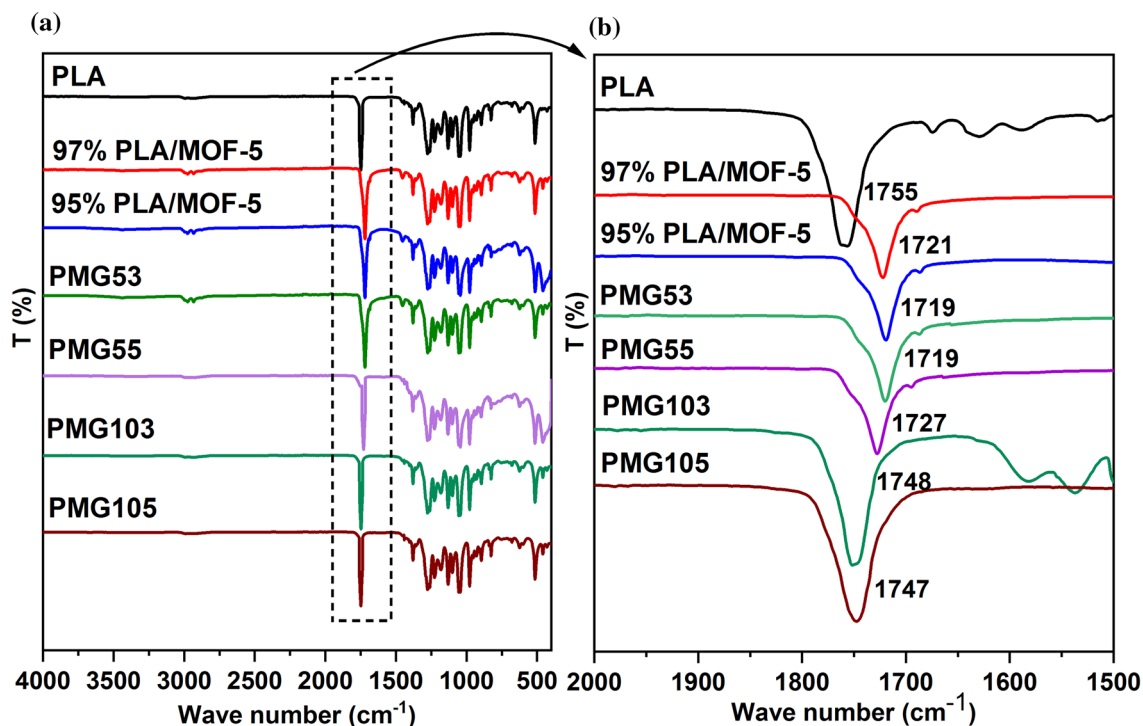
Fig. 2 FT-IR spectra of pure PLA, PLA/MOF-5, PMG5 and PMG10 materials

the polymer matrix. Figure 3 shows the XRD patterns of the PLA and PLA/MOF-5, PMG53, PMG55, PMG103, PMG105 nanocomposites. PLA shows a broad and characteristic peak at $2\theta = 16.4°$ attributed to the diffraction of (110)/(200) planes, suggesting the predominantly amorphous nature of the polymer [45].

Figure 3a shows the XRD patterns of GO, MOF-5 and MOF-5/GO. There is a strong peak at $2\theta = 10.85$ in GO pattern, which corresponds to (002) reflections of GO. The characteristic peaks of MOF-5 and MOF-5/GO marked in the figure are consistent with the literature as reported [29]. The XRD pattern of PLA/MOF-5 and PLA/MOF-5/GO nanocomposites show the presence of major peaks compared to the spectra of pure polymer and MOF-5 particles, indicating the preservation of the crystal in the polymer matrix and the change in the morphology of the polymer matrix as shown in Fig. 3. Minor changes in the intensity ratios were observed. The potential hydration of MOF-5 and the creation of certain phases of polymer matrix surrounding the inorganic nanofillers may be the cause of the shift in the intensity ratio of the peak corresponding to the (200) plane in the case of MOF-5 and PLA/MOF-5 [37, 46].

3.1.3 Scanning Electron Microscopy

Scanning electron microscopy (SEM) is used for an in-depth study of the structure of MOF-5 and MOF-5/GO fillers and

also for the study of the morphology of the different PLA matrix nanocomposites. Figure 4 shows the SEM image of the MOF-5 which will be used as nanofiller in this study. The particles have the appearance of a crystalline material with a particle size less than 500 nm. This observation is in a good agreement with the XRD analyses and confirms that the synthesis of MOF-5 produced a crystalline material (Fig. 3a).

Figure 5 presents the SEM images of PLA/MOF-5 and PLA/MOF-5/GO nanocomposites. The incorporation of the MOF-5 and MOF-5/GO (Fig. 5a–e) in PLA matrix clearly shows a more ductile fracture surface with a non-uniform MOF-5 distribution. The dispersion of the MOF-5 within the PLA matrix appears to be uniform, with agglomeration can be visualized (Fig. 5a). Similar phenomenon is observed for PLA/MD composites, in which slight agglomeration is reported at higher loadings [9].

However, when the MOF-5/GO was added to PLA, this trend is supplanted by the more uniform and regular dispersion of the nanoparticles everywhere throughout the matrix. From Fig. 5b–e, it can be seen that the MOF-5/GO particles are well-dispersed in the nanocomposites and no large agglomerates are observed, which indicates that the MOF-5/GO particles have excellent interface compatibility with PLA, even within the PLA matrix, suggesting that the nanoparticles are nominally attached to the polymeric matrix. Moreover, accumulation and aggregation are
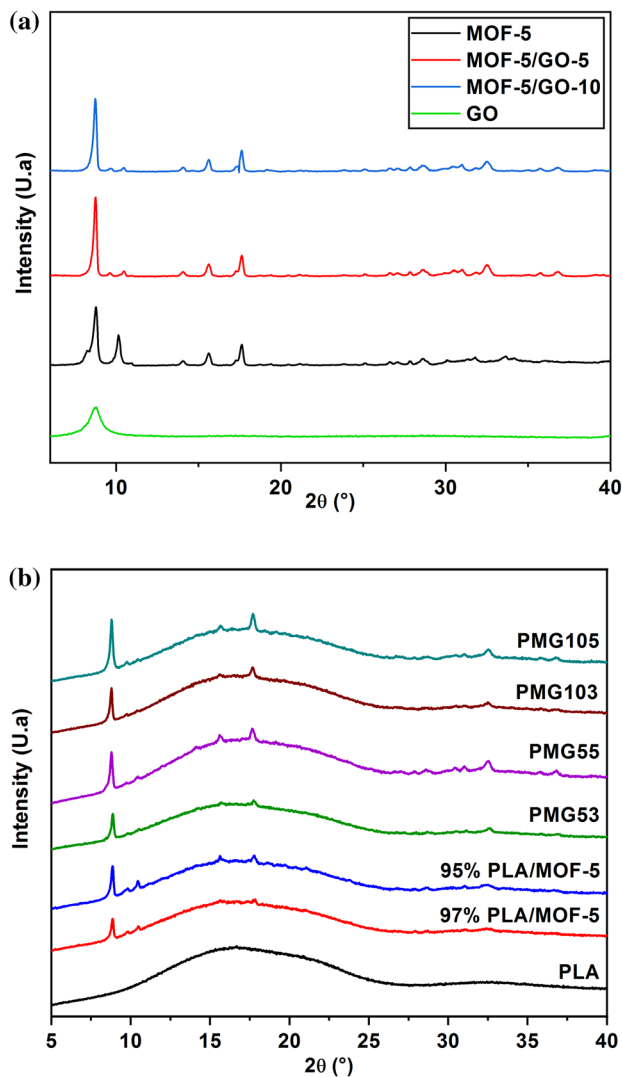
Fig. 3 XRD patterns of **a** MOF-5, MOF-5/GO-5 and MOF-5/GO-10 composites, and **b** pure PLA, PLA/MOF-5, PMG5 and PMG10 nanocomposites

not issues with PLA/MOF-5/GO nanocomposites [35, 36]. Zhang et al. conclude that the MOFs nanoparticles anchored on the GO sheets prevent GO from stacking together and make them disperse nicely in the PLA matrix [36]. Moreover, agglomeration and aggregation do not seem to be an issue with PLA/MOF-5/GO nanocomposites [46, 47]. Zhang et al. conclude that the MOFs nanoparticles anchored on the GO sheets prevent GO from stacking together and make them to disperse well in the PLA matrix [47].

3.1.4 Rheological Study

The rheological properties of nanocomposites based on polymer matrices are very sensitive to their multi-scale structure and strongly depend on the size, shape and also

the surface treatment of the reinforcements. Consequently, the rheometer is a tool of choice in order to characterize the dispersion state of nanofillers in polymer matrices.

Figure 6 represents the complex viscosity (η^*) vs frequency of PLA, PLA/MOF-5 and PLA/MOF-5/GO nanocomposites. The complex viscosity of the PLA matrix presents, as in the case of all unfilled polymers, a Newtonian plateau at low frequencies (Newtonian behavior) followed by a decrease in complex viscosity at higher frequencies. In the present work, a decrease of 44%, 25% and 52% of the complex viscosity was observed for PLA/MOF-5, PMG53 and PMG103 compared to PLA respectively, and also a decrease of 52.49% and 59% of the complex viscosity in the case of PMG55 and PMG105 compared to PLA respectively, which was inferred from increased free volume and decreased tangles. The decrease in complex viscosity of the composites compared to PLA can be attributed to the change in free volume and the decrease in entanglement as reported by Kathuria et al. [37] in their study of PLA/Cu_3BTC_2 composites where a decrease in the viscosity of the complex was obtained with the addition of Cu_3BTC_2 and attributed this phenomenon to the decrease in entanglement of linear polymer chains.

The storage modulus (G′) and loss modulus (G″) of PLA and PLA/MOF-5, PMG5 and PMG10 composites are shown respectively in Figs. 7 and 8. For pure PLA, G′ follows typical entangled polydisperse melt [48]. The G′ of the PLA/MOF-5 and PLA/MOF-5/GO composites show a gradual deviation in the slope of G′ at low frequencies with the formation of a secondary plateau or a terminal shoulder indicating the passage of a pseudo-liquid behavior towards a pseudo-solid behavior. This behavior was characteristic of the formation of a three-dimensional network caused by bridging of the strong polymer chain between MOF particles due to strong PLA/MOF-5 interactions. These topological constraints may have contributed to the immobilization of the polymer chains in the PLA/MOF-5 and PLA/MOF-5/GO composites, limiting their ability to relax at low frequencies. At high frequencies, the polymer chains were able to overcome these constraints. Similar rheological behaviors have been observed in polymer composites containing MOFs [49]. Adding 5% by weight of MOF-5/GO-5 to PLA causes an 8-fold increase in the storage modulus value compared to PLA, attributed to better particle dispersion in the PLA matrix. The variation of the loss modulus (G″), as a function of frequency of the PLA and its nanocomposites prepared with MOF-5 and MOF-5/GO, is illustrated in Fig. 8. The values of G″ exhibit a similar trend as G′, which is affected by the dispersion state of the incorporating nanofillers in the polymer matrix.

The tan δ (G″/G′) of PLA and PLA/MOF-5 and PLA/MOF-5/GO composites as a function of frequency is shown in Fig. 9a, b. This parameter, defined as the ratio of the
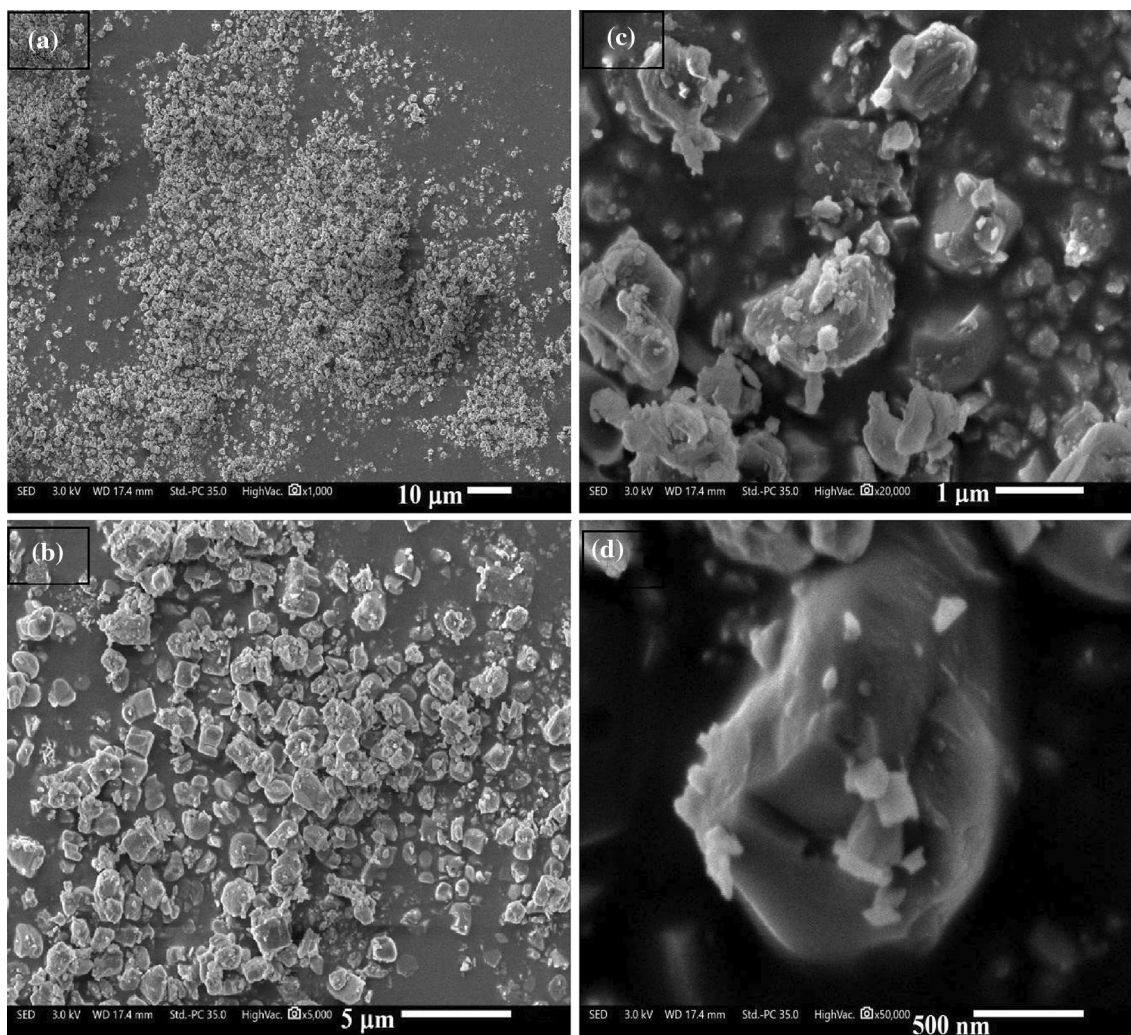
Fig. 4 SEM images of MOF-5 **a** scale size 10 μm, **b** scale size μm, **c** scale size 5 μm, and **d** scale size 500 nm

energy lost to the energy stored in a cyclic deformation (tan δ = G″/G′), is used here to compare the liquid-like versus solid-like behavior of PLA based materials. The PLA matrix shows a decrease of tan δ value with increasing frequency (negative slope), indicating a liquid-like behavior. It is seen that all nanofilled materials have comparable tan δ values at high frequencies but at low frequencies, energy dampening of the nanocomposites decreases and depends on the nanofiller nature and its concentration. Indeed, the curves of all hybrid samples demonstrate a positive slope due to their solid-like or elastic behavior [50, 51].

A Cole–Cole plot of PLA, PLA/MOF-5 and PLA/MOF-5/GO nanocomposites are shown in Fig. 10a, b. G′ and G″ represent the elastic and viscous parts of complex viscoelastic fluids. At low frequencies, the viscoelastic properties are very sensitive and indicative of the main molecular architecture of the MOF structure. At 175 °C, PLA exhibited mostly viscous behavior rather than elastic behavior.

However, with the addition of particles of MOF-5, MOF-5/GO-5 and MOF-5/GO-10, the elastic component of PLA increased at low frequencies with increasing filler content due to favorable interactions between the PLA matrix and MOF crystals [37].

3.2 Thermal Properties

3.2.1 Differential Scanning Calorimetry Analysis

Differential scanning calorimetry (DSC) consists of measuring the heat flux necessary to maintain a sample at the same temperature as a reference during heating or cooling. Figure 11 represents DSC analysis results for PLA, PLA/MOF-5 and PLA/MOF-5/GO nanocomposites and the results values are summarized in Table 1.

The crystallization onset temperatures for 97% PLA/MOF-5, 95% PLA/MOF-5, PMG53, PMG55, PMG103
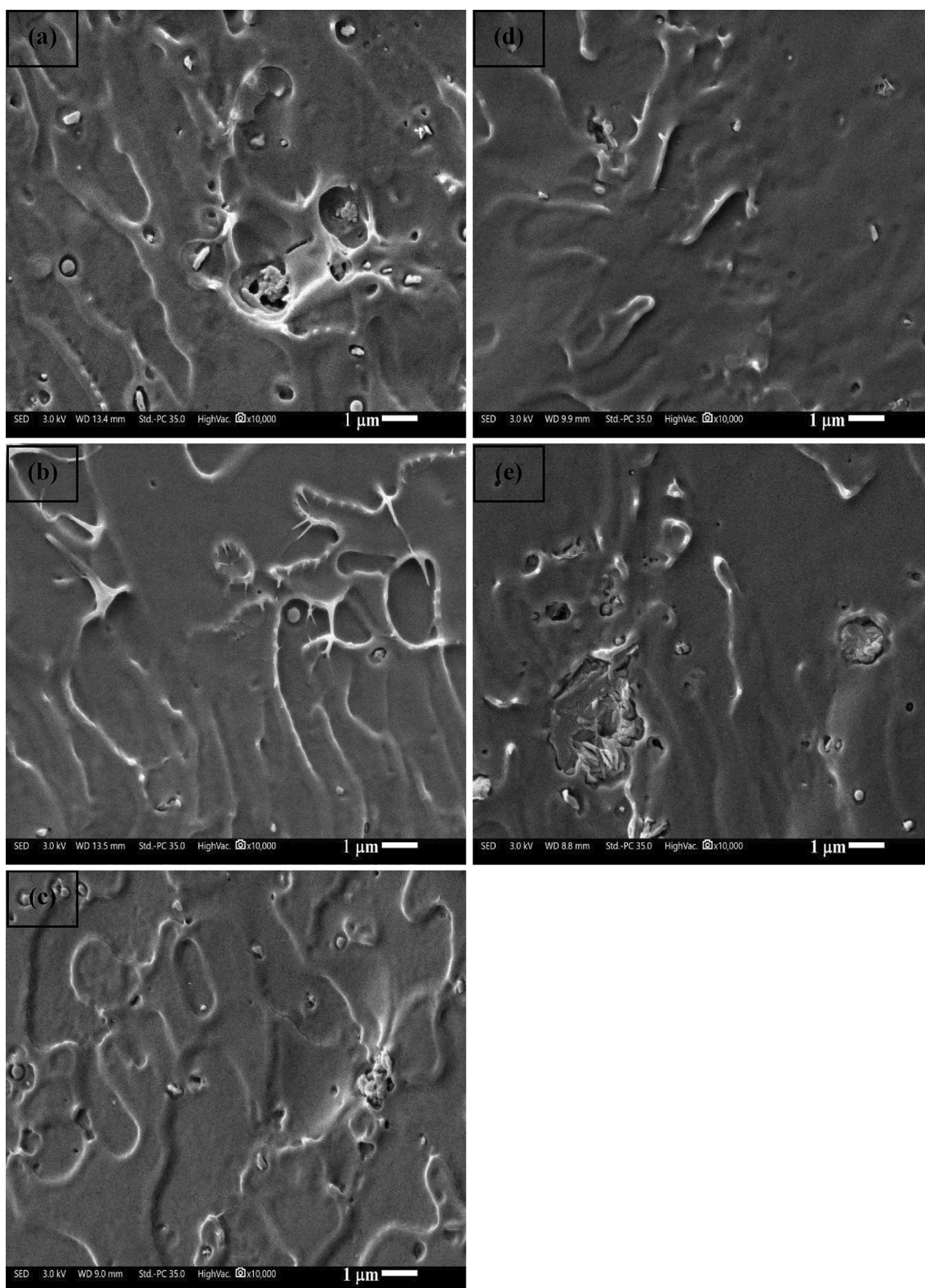
Fig. 5 SEM images with scale size 1 μm of **a** PLA/MOF-5, **b** PMG53, **c** PMG55, **d** PMG103 and **e** PMG10
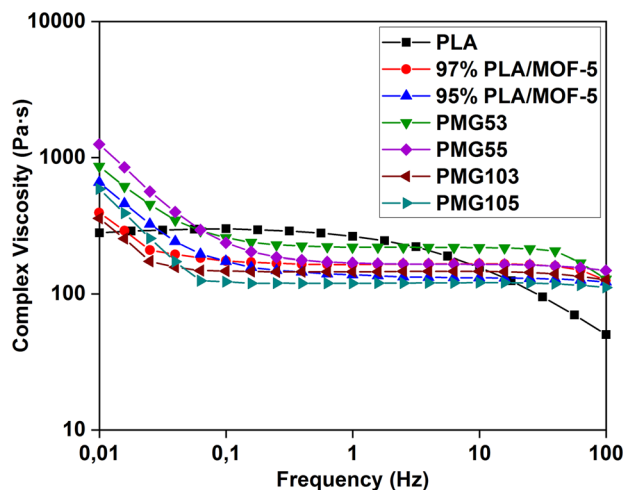
Fig. 6 Complex viscosity of pure PLA, PLA/MOF-5 and PLA/MOF-5/GO nanocomposites

and PMG105 observed in DSC tests were 111.08, 107.29, 106.15, 108.56, 106.48 and 107.5 °C, respectively. The shift in crystallization onset temperature of PLA/MOF-5 nanocomposites to higher temperatures with increasing MOF-5 and MOF-5/GO content can be attributed to the good interactions between polymer chains of PLA and MOF-5 crystals [52]. We can also observe that the cold crystallization enthalpy was increased with the addition of MOF-5 and MOF-5/GO. It must be noticed that glass temperature (T_g) of PLA is located at 59.4 °C and there was no significant change in the T_g of the composites compared to PLA, indicating that the addition of MOF-5 and MOF-5/GO crystals does not provide any flexibility to the chain. So, the presence of nanofillers in the PLA matrix does not improve its crystallinity rate as presented in Table 1. The value of the crystallinity rate (X_c) is obtained using Eq. (1).

3.2.2 Thermogravimetric Analysis (TGA)

The thermal stability of PLA based nanocomposites was studied by TGA under a nitrogen flow at a heating rate of 10 °C/min. The typical curves of the TGA for pure PLA and its nanocomposites are presented in Fig. 12 and the global results are gathered in Table 2. The parameter which seems to be the most important to characterize the thermal stability is the onset temperature of degradation, which is measured by the temperature at which 5% mass loss occurs ($T_{5\%}$).

The decomposition of PLA occurs in a one-step process, with a degradation temperature of 306.7 °C. It should be noticed that about 95% of the decomposition takes place at 361 °C [35]. PLA/MOF-5 nanocomposites show degradation similar to that of pure PLA. However, it appears that the degradation temperatures of the nanocomposites are lower than those of the both PLA and MOF-5. Indeed, the average
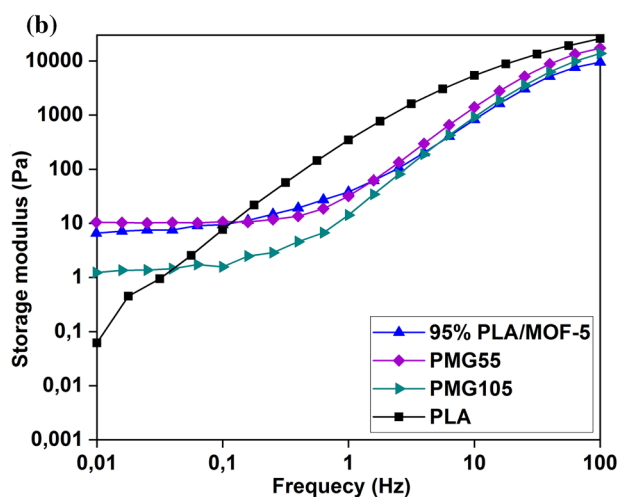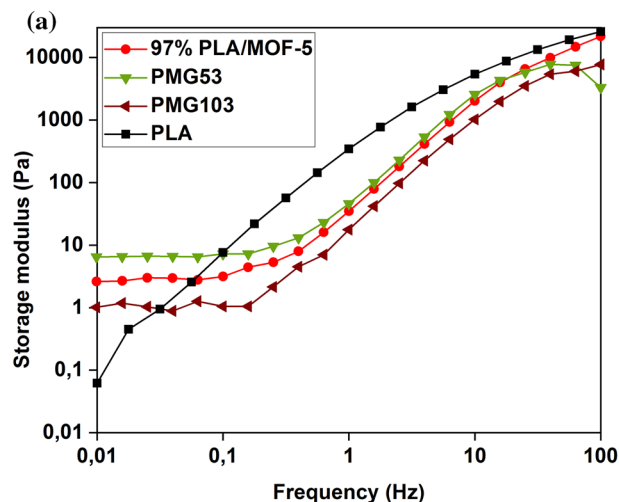

Fig. 7 Storage modulus of **a** pure PLA, 97% PLA/MOF-5, PMG53 and PMG103 nanocomposites and **b** pure PLA, 95% PLA/MOF-5, PMG55 and PMG105 nanocomposites as a function of oscillatory frequency

onset of thermal decomposition of 97% PLA/MOF-5 and 95% PLA/MOF-5 are 304 °C and 293 °C, respectively [35]. This could be attributed to the conversion of the remaining benzene carboxylates groups present in the MOF into CO and CO_2. The difference in the final plateau for PLA, 97% PLA/MOF-5 and 95% PLA/MOF-5 is mainly attributed to the difference in the metal content of the composites. While, increasing the concentration of MOF-5/GO-5 increases the onset of thermal degradation of nanocomposites. Indeed, the decomposition temperatures for PMG53 and PMG55 were respectively 303.98 °C and 311.33 °C.

3.3 Impact Resistance Tests

The results of Izod impact strength analysis of PLA, PLA/MOF-5 and PLA/MOF-5/GO nanocomposites are shown
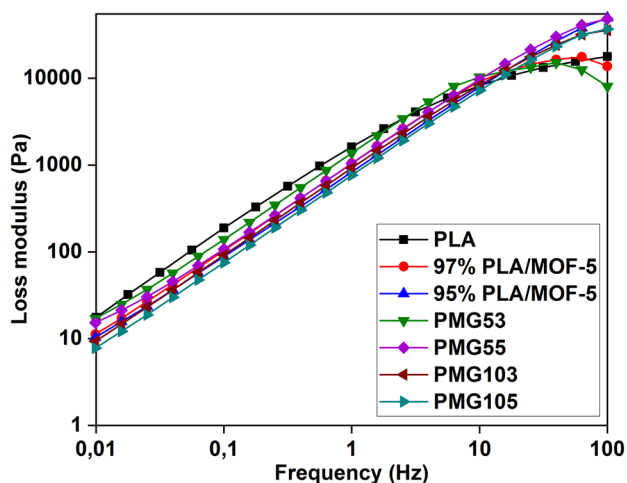
Fig. 8 Loss modulus of pure PLA, PLA/MOF-5 and PLA/MOF-5/GO nanocomposites as a function of oscillatory frequency
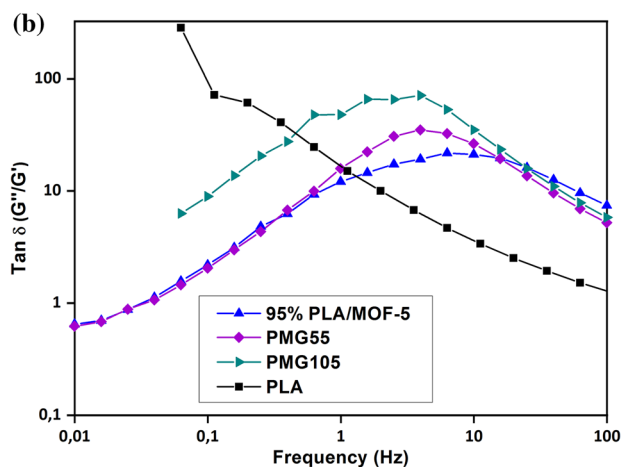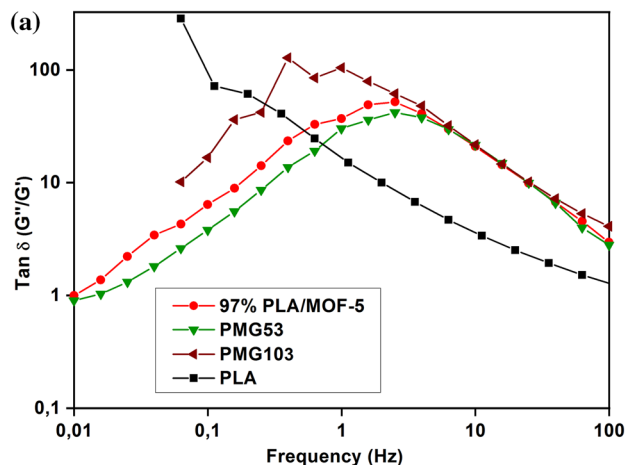

Fig. 9 tan δ curves of **a** pure PLA, 97% PLA/MOF, PMG53 and PMG103 nanocomposites and **b** pure PLA, 95% PLA/MOF, PMG55 and PMG105 nanocomposites
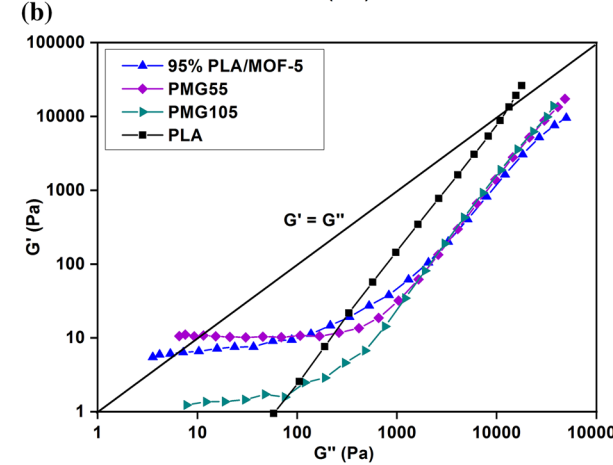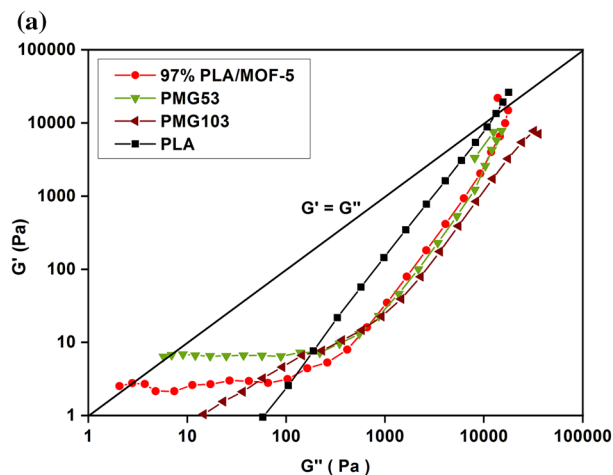

Fig. 10 Cole–Cole plot of **a** pure PLA, 97% PLA/MOF-5, PMG53 and PMG103 composites, and **b** pure PLA, 95% PLA/MOF-5, PMG55 and PMG105 composites
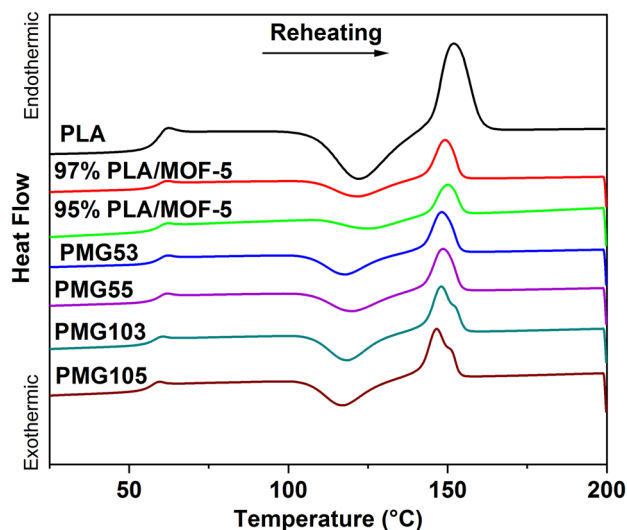

Fig. 11 DSC thermograms of the pure PLA and its nanocomposites PLA/MOF-5 and PLA/MOF-5/GO

Table 1 Thermal parameters obtained by DSC for PLA and its nanocomposites

Sample	T_g (°C)	Cold crystallization			Melting			X_c (%)
		T_{c0} (°C)	T_{cc} (°C)	ΔH_c (J/g)	T_{m0} (°C)	T_m (°C)	ΔH_m (J/g)	
PLA	59.4	–	122.2	–	–	151.9	24.92	26.6
97% PLA/MOF-5	59.84	108.56	122.07	−13.53	143.35	149.19	14.76	16.26
PMG53	59.81	106.48	117.90	−14.88	142.36	148.19	16.55	18.23
PMG103	58.09	107.50	118.52	−17.85	142.58	148.07	20.09	22.13
95% PLA/MOF-5	59.79	111.08	126.21	−8.56	144.47	150.15	10.42	11.47
PMG55	59.87	107.29	120.26	−15.25	142.80	148.56	16.78	18.48
PMG105	57.49	106.15	117.13	−18.66	141.49	146.57	20.13	22.17

Fig. 12 TGA curves of pure PLA and it nanocomposites PLA/MOF-5, PMG5 and PMG10
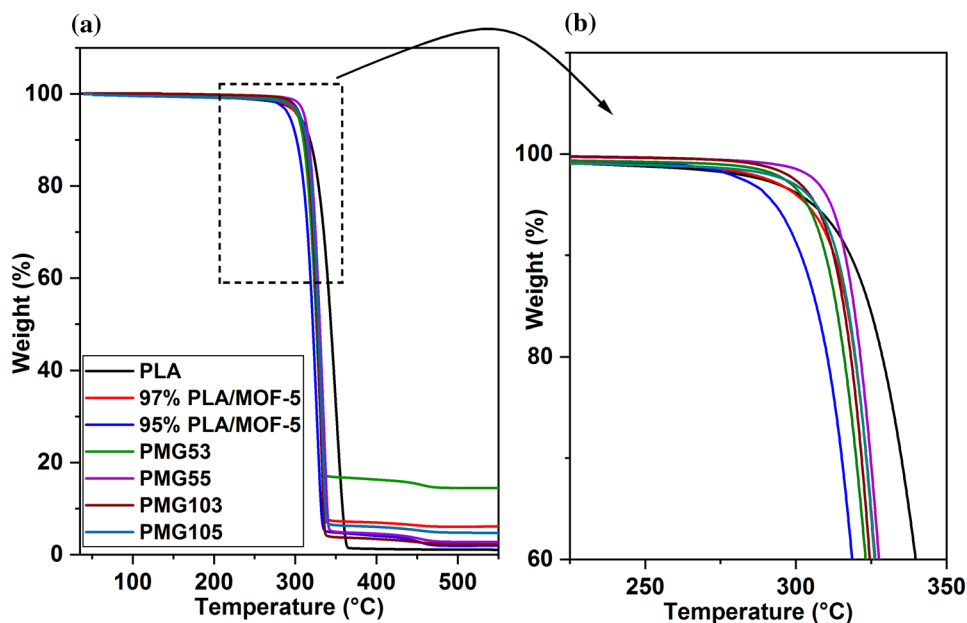
Table 2 TGA parameters of pure PLA, PLA/MOF-5 and PLA/MOF-5/GO nanocomposites

Sample	$T_{5\%}$ (°C)	$T_{50\%}$ (°C)
PLA	306.7	343.22
97% PLA/MOF-5	303.98	328.24
95% PLA/MOF-5	293.13	321.54
PMG53	303.98	325.69
PMG55	311.33	330.13
PMG103	301.97	326.97
PMG105	307.97	328.24

Table 3 Impact test results for pure PLA and its nanocomposites

Materials	Energy (J/m)
PLA	0.464 ± 0.01
97% PLA/MOF-5	0.359 ± 0.04
95% PLA/MOF-5	0.354 ± 0.01
PMG53	0.436 ± 0.03
PMG55	0.557 ± 0.04
PMG103	0.521 ± 0.04
PMG105	0.689 ± 0.05

in Table 3. It had a difference in impact resistance between PLA and PLA nanocomposites at 3 and 5 wt% MOF-5. The addition of MOF-5 results a decrease in impact resistance (decrease in the energy needed to destroy a highlight). It can therefore be concluded that the MOF-5 has weakened the PLA. However, in the case of PLA nanocomposites containing 3 and 5% of MOF-5/GO, the impact resistance increases with increasing amounts of MOF-5/GO nanofillers. This result clearly shows that the addition of GO reinforces the PLA and it may be explained by the MOF-5/GO has a large surface area, which can absorb a significant amount of the impact energy, and the voids functioning as an impact cushion.

Table 4 Water vapor permeability

Materials	PVE * 10^{-11} (g/m s Pa)
PLA	3.036 ±0.01
97%PLA/MOF-5	2.95 ±0.01
95% PLA/MOF-5	2.91 ±0.01
PMG53	2.68 ±0.01
PMG55	2.06 ±0.01
PMG103	2.53 ±0.01
PMG105	2.02 ±0.01

3.4 Water Vapor Permeability Test

The water vapor permeability (WVP) properties of polymer nanocomposites depend on the polymer matrix, the MOF crystals and the final morphology of the composites. Therefore, with varying interfacial interactions between the polymer matrix and the porous filler, the polymer nanocomposites can exist in five different morphologies: (1) the ideal two-phase morphology without defect or distortion, which exists under good interfacial interactions between the polymer and the filler porous. (2) The incompatibility between the polymer and the filler, which results in voids at the interface. (3) The dilated interface, which may be the result of the low density of the polymer chain around the filler. (4) The densely packed polymeric zone present around the interface due to strong interactions. (5) In addition, it is also possible to have a clogged charge, which can form during the manufacture of polymer nanocomposites [36].

The WVP coefficients of the PLA matrix and hybrid materials are shown in Table 4. The results clearly show that the addition of MOF-5 to PLA causes a slight decrease in WVP values. These results are in good agreement with that obtained by Kathuria et al. [36] which found that the addition of MOF does not influence the WVP of PLLA. The addition of the GO to the MOF-5 crystals considerably reduced the WVP coefficients of the PLA matrix. Indeed, the PVE of PLA decreases from 3.036 to 2.06 and 2.02 in the case of PMG55 and PMG105 nanocomposites, respectively. Such a trend confirms that the addition of GO in the polymer matrices has an obvious effect on their gas permeability, as shown by the WVP [53]. This decrease is due to the good dispersion of the MOF-5/GO-5 and MOF-5/GO-10 nanofillers compared to the MOF-5 confirmed by the SEM analysis and rheological measurements.

4 Conclusion

In summary, PLA/MOF-5 and PLA/MOF-5/GO nanocomposites were prepared using melt extrusion method by a vertical co-rotating twin screw micro compounder and its packaging properties are investigated. The XRD analysis confirmed the slight enhancement in the crystallinity (%) for PLA/MOF-5 and PLA/MOF-5/GO nanocomposites and MOF-5 retained their structure during extrusion processing. SEM and XRD confirmed that the nanofillers are present on the film surface. Favorable interfacial interactions necessary between MOF-5, MOF-5/GO and PLA for improved toughening were further endorsed by rheological, microscopy studies and thermal analysis (DSC studies). The TGA analysis revealed that the incorporation of MOF-5 and MOF-5/GO composites shows slight reduction in T_{max} for PLA. The presence of MOF-5 and MOF-5/GO nanofillers in the PLA matrix, especially MOF-5/GO-5 filler, can significantly influence the barrier properties of water vapor providing a gamut of opportunities in several application fields. Packaging, especially food packaging and photocatalysis are the most considered areas for this type of materials with modulated barrier properties. However, the study of the toxicity of all nanoparticles as well as their migration phenomena when they are in contact with food is necessary.

Declarations

References

1. B.S. Bouakaz, A. Habi, Y. Grohens, I. Pillin, Appl. Clay Sci. **139**, 81 (2017)
2. B.W. Chieng, N.A. Ibrahim, W.M.Z. Wan Yunus, M.Z. Hussein, Y.Y. Loo, J. Therm. Anal. Calorim. **118**, 1551 (2014)
3. G. Huang, S. Chen, P. Song, P. Lu, C. Wu, H. Liang, Appl. Clay Sci. **88–89**, 78 (2014)
4. K. Issaadi, A. Habi, Y. Grohens, I. Pillin, Polym. Bull. **73**, 2057 (2016)
5. S. Adrar, A. Habi, A. Ajji, Y. Grohens, Appl. Clay Sci. **146**, 306 (2017)
6. A. Chakraborty, P. Ghalsasi, P. Radha, J. Inorg. Organomet. Polym. Mater. **33**, 1119 (2023)
7. F. Chen, X. Ni, Y. Liu, X. Xia, X. Gao, J. Mater. Sci. **57**, 14819 (2022)
8. Z.A. Raza, H. Akram, I.A. Bhatti, J. Inorg. Organomet. Polym. Mater. **33**, 151 (2023)
9. U. Lawal, V. Robert, S. Loganathan, R.B. Valapa, J. Polym. Environ. **31**, 1938 (2023)
10. A. Nadernezhad, S. Unal, N. Khani, B. Koc, Int. J. Adv. Manuf. Technol. **102**, 2119 (2019)
11. B.S. Bouakaz, I. Pillin, A. Habi, Y. Grohens, Appl. Clay Sci. **116–117**, 69 (2015)
12. F. Mai, Y. Habibi, J.-M. Raquez, P. Dubois, J.-F. Feller, T. Peijs, E. Bilotti, Polymer **54**, 6818 (2013)

13. K. Issaadi, A. Habi, Y. Grohens, I. Pillin, Appl. Clay Sci. **107**, 62 (2015)
14. N. Nath, S. Chakroborty, P. Panda, K. Pal, Top. Catal. **65**, 1706 (2022)
15. K. Issaadi, I. Pillin, A. Habi, Y. Grohens, Polym. Bull. **74**, 997 (2017)
16. W. Tighzert, A. Habi, A. Ajji, T. Sadoun, F.B.-O. Daoud, Fibers Polym. **18**, 514 (2017)
17. K. Pal, S. Chakroborty, P. Panda, N. Nath, S. Soren, Environ. Sci. Pollut. Res. **29**, 76626 (2022)
18. D. Saaoui, S. Benali, R. Mincheva, A. Habi, P. Dubois, J. Raquez, J. Appl. Polym. Sci. **137**, 48812 (2020)
19. A. Habi, S. Djadoun, Y. Grohens, J. Appl. Polym. Sci. **114**, 322 (2009)
20. F. Benhacine, A.S. Hadj-Hamou, A. Habi, Y. Grohens, Int. Polym. Process. **30**, 511 (2015)
21. K. Pal, N. Asthana, A.A. Aljabali, S.K. Bhardwaj, S. Kralj, A. Penkova, S. Thomas, T. Zaheer, F. Gomes de Souza, Crit. Rev. Solid State Mater. Sci. **47**, 691 (2022)
22. K. Pal, A.A. Aljabali, S. Kralj, S. Thomas, F. Gomes de Souza, Chemosphere **263**, 128104 (2021)
23. K. Pal, A. Si, G.S. El-Sayyad, M.A. Elkodous, R. Kumar, A.I. El-Batal, S. Kralj, S. Thomas, Crit. Rev. Solid State Mater. Sci. **46**, 385 (2021)
24. N. Nath, A. Kumar, S. Chakroborty, S. Soren, A. Barik, K. Pal, F.G. De Souza, ACS Omega **8**, 4436 (2023)
25. S. Bagyalakshmi, A. Sivakami, K. Pal, R. Sarankumar, C. Mahendran, J. Nanopart. Res. **24**, 201 (2022)
26. F. Gao, F. Wu, X. Zhang, B. Jiang, Q. Li, J. Inorg. Organomet. Polym. Mater. **33**, 328 (2023)
27. Y. Cao, Y. Zhao, Z. Lv, F. Song, Q. Zhong, J. Ind. Eng. Chem. **27**, 102 (2015)
28. D. Damasceno Borges, P. Normand, A. Permiakova, R. Babarao, N. Heymans, D.S. Galvao, C. Serre, G. De Weireld, G. Maurin, J. Phys. Chem. C **121**, 26822 (2017)
29. B. Bouider, S. Haffad, B.S. Bouakaz, M. Berd, S. Ouhnia, A. Habi, J. Inorg. Organomet. Polym. Mater. (2023). https://doi.org/10.1007/s10904-023-02668-y
30. D.J. Tranchemontagne, J.R. Hunt, O.M. Yaghi, Tetrahedron **64**, 8553 (2008)
31. Kirandeep, J. Kaur, I. Sharma, E. Zangrando, K. Pal, S.K. Mehta, R. Kataria, J. Mater. Res. Technol. **22**, 278 (2023)
32. L. Zhu, H. Yu, H. Zhang, J. Shen, L. Xue, C. Gao, B. van der Bruggen, RSC Adv. **5**, 73068 (2015)
33. C. Petit, T.J. Bandosz, Adv. Mater. **21**, 4753 (2009)
34. A. Kathuria, N. Brouwers, M. Buntinx, T. Harding, R. Auras, J. Appl. Polym. Sci. **135**, 45690 (2018)
35. Y. Wang, X. Dai, X. Li, X. Wang, Mater. Res. Express **5**, 036416 (2018)
36. A. Kathuria, S. Al-Ghamdi, M.G. Abiad, R. Auras, J. Appl. Polym. Sci. **132**, 42764 (2015)
37. A. Kathuria, M.G. Abiad, R. Auras, Polymer **54**, 6979 (2013)
38. A. Kathuria, M.G. Abiad, R. Auras, Polym. Int. **62**, 1144 (2013)
39. X. Dai, X. Li, M. Zhang, J. Xie, X. Wang, ACS Omega **3**, 6860 (2018)
40. X. Dai, Y. Cao, X. Shi, X. Wang, Adv. Mater. Interfaces **3**, 1600725 (2016)
41. W.S. Hummers, R.E. Offeman, J. Am. Chem. Soc. **80**, 1339 (1958)
42. S.N. Alam, N. Sharma, L. Kumar, Graphene **06**, 1 (2017)
43. S. Wang, B. Ye, C. An, J. Wang, Q. Li, H. Guo, J. Zhang, Nanoscale Res. Lett. **14**, 345 (2019)
44. X. Dai, Y. Cao, X. Shi, X. Wang, RSC Adv. **6**, 71461 (2016)
45. I. Athanasoulia, K. Giachalis, D. Korres, N. Todorova, T. Giannakopoulou, P.A. Tarantili, C. Trapalis, Polym. Int. **69**, 995 (2020)
46. V. Nafisi, M.-B. Hägg, Sep. Purif. Technol. **128**, 31 (2014)
47. M. Zhang, X. Shi, X. Dai, C. Huo, J. Xie, X. Li, X. Wang, J. Mater. Sci. **53**, 7083 (2018)
48. R.N. Darie, E. Pâslaru, A. Sdrobis, G.M. Pricope, G.E. Hitruc, A. Poiată, A. Baklavaridis, C. Vasile, Ind. Eng. Chem. Res. **53**, 7877 (2014)
49. J.-Y. Choi, J. Kim, S.-H. Jhung, H.-K. Kim, J.-S. Chang, H.K. Chae, Bull. Korean Chem. Soc. **27**, 1523 (2006)
50. B.S. Bouakaz, A. Habi, Y. Grohens, I. Pillin, Appl. Clay Sci. **161**, 35 (2018)
51. K. Rinawa, S.N. Maiti, R. Sonnier, J.-M. Lopez Cuesta, Polym. Bull. **72**, 3305 (2015)
52. Y. Ming, N. Kumar, D.J. Siegel, ACS Omega **2**, 4921 (2017)
53. J.-H. Chang, Y.U. An, G.S. Sur, J. Polym. Sci. B **41**, 94 (2003)